Power Distribution and Thermal Management Modeling for Electrified Aircraft

Saakar Byahut* and Alejandra Uranga†
University of Southern California, Los Angeles, CA 90089, USA

Despite the substantially lower energy per unit mass of batteries compared to hydrocarbon fuels, electrification of the aircraft propulsion system could lead to increases in energy efficiency for certain types of missions. This work builds on the electric powertrain component models (battery, converter, motor) from previous work and presents models for the propulsor, power distribution system, thermal management system (TMS), and wiring in order to complete an all-electric propulsion system framework. This framework is used to simulate a propulsion system with power loads representative of a commuter aircraft mission that transports 19 passengers over 100 nmi. Results show that the battery makes up over 60% of the total propulsion system mass, indicating that improvements in battery technology are essential to lower propulsion system mass. Despite making up a smaller fraction of the propulsion system mass, the other components impact the overall system via their efficiency since that sizes the battery and the TMS. Distributed propulsion is found to lower the propulsion system mass, with diminishing returns beyond 10 propulsors due to the increased heat rejection and hence TMS mass.

I. Introduction

A. Motivation and Background

To balance the steady growth in demand for air transportation with the increasing emphasis on environmental sustainability, the aircraft design space has been opened up for novel architectures which could contribute to higher energy efficiency for commercial aircraft. Aircraft using electrical components for propulsion, or *electrified aircraft*, present one promising path towards energy efficiency gains.

Electrification of the aircraft propulsion system can take advantage of the higher component efficiencies, and synergize with benefits from distributed propulsion (DP) and boundary layer ingestion (BLI) to provide energy usage benefits over current hydrocarbon-burning aircraft [1, 2]. However, electrification comes with its own set of challenges. Foremost, state-of-the art battery packs currently have specific energies (energy per unit mass) of about 175 Wh/kg – two orders of magnitude smaller than that of hydrocarbon fuels (roughly 13 000 Wh/kg). Even with substantial improvements, batteries are unlikely to attain specific energies comparable to hydrocarbon fuels used in aviation. Hence, substituting an electrified propulsion system in place of a conventional system is not expected be practical because of the additional weight and complexity [3]. Rather, novel designs require the reconfiguration of the full aircraft in order to leverage the higher power delivery efficiencies associated with electrical components, as well as to take advantage of the additional benefits offered by DP and BLI.

Previous work by the authors [1, 2] explored the design space with low-fidelity electrical component models and analyzed both electrified and conventional aircraft over cruise-only missions spanning payloads and ranges of commercial aircraft. The effects of different technology assumptions for electrical components were examined, as were the contributions to energy efficiency from DP and BLI. Those results showed energy-usage benefits for electrified aircraft, especially for smaller aircraft flying short missions. All-electric commuter (thin-haul) aircraft, carrying 19 passengers over 100 nautical miles (nmi), were found to be feasible in terms of technology levels expected within the next decade or so, and provide energy-usage benefits. However, those results were found to be highly sensitive to electrical component technology levels. In addition, due to the nature of the cruise-only analysis, the behavior of electrical components under the different power loads across various flight segments could not be examined.

Subsequent work [4] modeled electrical components at a higher fidelity, which captured their behavior for the variable power demands of different flight segments. Results showed that the higher-fidelity models predict higher

---

energy requirements for the mission. The component efficiencies change when operated at off-design conditions. Distributed propulsion also changes the system efficiency at lower power levels. However, these models also predicted very high system voltages, orders of magnitude beyond where arcing occurs. These voltages are not practical without a high-voltage power distribution system, and/or constraints for maximum allowable voltage for safety and wiring protection concerns. In addition, that work focused on the powertrain part of the propulsion system, namely the battery, motor, and converter. The varying efficiencies of the electrical components across different power levels required during the flight necessitated a thermal management system (TMS) to handle wasted energy dissipated as heat.

B. Scope

A definite conclusion of whether electrification makes sense for specific mission requires a targeted effort into understanding the performance characteristics of the electric propulsion system and its components. This analysis can only be done with higher-fidelity representations of the propulsion system components, particularly with regard to masses and efficiencies. This paper builds on previous work on the propulsion powertrain [4] and forms a complete propulsion *system* by modeling additional components — namely TMS, power distribution, wiring, and the propulsor. These models capture operational behavior of the components across varying power levels at different flight segments, Together with the powertrain components (battery, motor, converter) from previous work, this work integrates all of these models into an all-electric propulsion system for a commuter aircraft mission.

The propulsion system is then sized in terms of mass based on the energy and power requirements for the mission. The results quantify the masses of the components as well as the overall propulsion system, and the energy and maximum power demands. The effects of distributed propulsion are analyzed, and the differences are explained in terms of operational behavior.

C. Terminology

The term *all-electric* here refers to a propulsion system architecture where all the energy needed for propulsion is stored in batteries. An all-electric architecture consists of a power delivery chain from the batteries to a converter, which powers an array of motors, each driving a propulsor (typically a fan), along with the necessary power distribution including wiring, and TMS. The mission considered here is that of a *commuter aircraft*, carrying a payload of 19 passengers over 100 nmi. The Viking Air Twin Otter is a representative commuter aircraft that serves as the conventional baseline for the analysis.

For an all-electric aircraft, the propulsion *powertrain* includes the power-converting components of the propulsion system: battery, converter, and motor. These components were modeled as part of a previous work [4]. The propulsion *system* includes the powertrain, as well as the additional components required for power delivery: power distribution system, wiring, and TMS, as well as the propulsor that converts the electrical power into flow power.

II. Component Models

Models for the battery, converter, and motor were introduced in a previous work [4] and will be reused here. The battery model simulates capacity discharge using a nearly-linear set of equations and uses them to size the battery based on the aircraft energy and power requirements at each flight segment. The motor is a switched reluctance motor and the converter is a DC-DC transformer. Both are modeled incorporating power losses due to resistive as well as core elements, and sized based on the maximum power required for the flight.

The propulsion system also includes wiring and a power distribution system to deliver power from the batteries through the converter to the motors. To complete the power delivery chain, a propulsor model converts the mechanical shaft power from the motor to the flow power. In addition, because the components do not operate at 100% efficiency, a thermal management system is needed to deal with the heat loss. This section presents models for the propulsor, power distribution, wiring, and thermal management. Together with the models previously presented [4], this completes the entire all-electric propulsion system framework.

A. Propulsor

Since this work focuses on commuter aircraft, it is assumed that the propulsor is a propeller, in order to provide a relevant comparison with conventional aircraft like the Twin Otter. The propulsor model is then incorporated as a

scaling law [5] that sets the mass (in kg) of each propeller as

$$m_{\text{prop}} = k_{\text{prop}} \left(D_{\text{prop}} P_{\text{TO}} \sqrt{B_{\text{prop}}} \right)^{0.782}, \tag{1}$$

where D_{prop} is the propeller diameter in meters, P_{TO} is the takeoff power per propulsor in horsepower, B_{prop} is the number of blades per propeller, and $k_{\text{prop}} = 0.124$ is a scaling constant with appropriate units.

The nacelle is also sized using a scaling law [5] based on the equivalent shaft horsepower, ESHP, of the engine in the conventional case and the motor shaft power for all-electric aircraft. The nacelle mass is then computed as

$$m_{\text{nace}} = k_{\text{nace}} \times \text{ESHP}, \tag{2}$$

where $k_{\text{nace}} = 0.0635 \, \text{kg/hp}$ is a scaling constant.

B. Power Distribution

The power distribution system is a combination of a converter that takes power from the battery, transforms it to the voltage optimal for transmission, and distributes it to the motor-propulsor arrays. For a propulsion system with N_{prop} propulsors, there is an equivalent number of motor-propulsor arrays; each of those receive power from the converter. In previous work [4], it was thought that the array consisted of converters, motors, and propulsors, but the results indicated system voltages about two orders of magnitude beyond the breakdown voltage set by Paschen's Law [6]. Operating at voltages beyond this limit compromises the safety and functionality of the electrical components and power distribution due to the risk of arcing and discharge through the air. Therefore, such high voltages are not representative of a practical system.

These voltages require safe distribution of power, as well as safety limits in case the voltages are beyond any limits prescribed by certification requirements, physical and operational constraints. Therefore, in this work, instead of there being N_{prop} converters, there is now only one converter that forms the integral part of the power distribution system. This converter steps up the battery voltage to a voltage suitable for safe transmission, and thus transfers power to the motor-propulsor arrays. In this sense, this modeling approach assumes that each motor includes an appropriate controller required for it.

To set limits for power distribution, it is important to look at the voltage limits set by physics and by operational constraints. Paschen's Law [7] gives the breakdown voltage, or the voltage required to create a discharge or an electric arc between two electrodes in a gas in terms of the pressure p and the separation between the electrodes d,

$$V_{\text{bd}} = \frac{B \, pd}{\ln \left[\dfrac{A \, pd}{\ln \left(1 + \frac{1}{\gamma} \right)} \right]}, \tag{3}$$

where for air, the constants $A = 11.25 \, \text{Pa}^{-1}\text{m}^{-1}$, $B = 273.75 \, \text{V} \, \text{Pa}^{-1}\text{m}^{-1}$, and $\gamma = 0.011$ is the secondary ionization coefficient. Figure 1 plots the breakdown voltage on a logarithmic scale as a function of the product of pressure and gap length pd. It can be seen that this curve shows a minimum breakdown voltage of $V_{\text{bd}} = 327 \, \text{V}$ at $pd = 0.760 \, \text{Pa·m}$, indicating that this voltage is the absolute worst case for any product of pressure and distance. Specifically for aircraft, system voltages less than 327 V, such the current standard of 270 V used in military aircraft [8], or the ±270 VDC in the Boeing 787 [6], should never have arcing or partial discharge issues.

However, since the curve is plotted as a function of the product pd, a minimum breakdown voltage of 327 V corresponds to a spacing of only 7.5 μm at sea-level pressure of 1 atm, and a spacing of about 0.05 mm at a pressure of 0.16 atm at the service ceiling of 43,000 ft [9] for large, long-range aircraft like the Boeing 777 or Airbus A350. Such separation distances are impractical. Furthermore, with increased separation, the breakdown voltage increases beyond the absolute minimum of 327 V.

In addition, Eqn. (3) applies to two uninsulated conductors, whereas, for most wiring, the conductors are sheathed using insulation usually made up of plastic materials. The fraction of the wire voltage across the air gap for insulated conductors [6] is given by

$$f_V = \frac{d}{d + \frac{t_i}{\varepsilon_r}}, \tag{4}$$

3
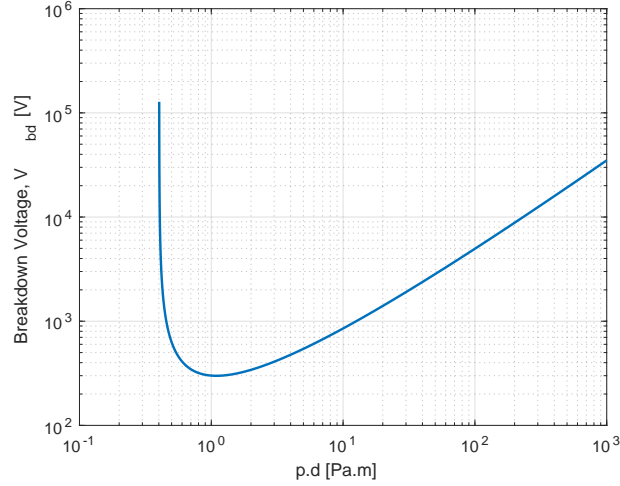
Fig. 1 Paschen's curve for air.

where t_i and ε_r are the thickness and dielectric constant of the insulation material, respectively. Using this fraction, a safe operating voltage, SOV, can be calculated as

$$\text{SOV} \;=\; \frac{V_{\text{bd}}}{f_V} \,.\tag{5}$$

With insulation and an increased separation between conductors, the SOV can be much higher than the absolute lowest limit from Paschen's Law. On the other hand, applying a safety factor of 1.2 as is common for power transmission [10] or of 1.5 as normally used in aerospace yields a lower SOV. However, this limit can be used with more confidence in order to account for transient effects and surges.

C. Cables and Wiring

To mitigate the effects of high voltages, cables and wiring design also have to be considered. A safe operating voltage for the aircraft is calculated based on the maximum operating altitude, the separation between wires, the wiring thickness, and the insulation material. Since the wires primarily supply power to the motor from the power distribution system, they are sized based on the maximum power they need to handle, and the SOV. The standard electrical power equation,

$$P \;=\; IV \,,\tag{6}$$

is used with $P = P_{\text{mot,in}}$ the input power to each motor, $V = \text{SOV}$, and I the current through the wires. Wires can be selected from standard diameters from the American Wire Gauge (AWG), based on the maximum current that needs to flow through them.

A direct current (DC) system, in line with previously-developed models for the motor and the converter [4], typically uses four wires, with one wire each carrying the positive and negative voltages and two ground wires [6]. Depending on the material of the wires (typically copper or aluminum), its resistance can be calculated from its dimensions and the conductivity of the material as

$$R_{\text{cable}} \;=\; \frac{L_{\text{cable}}}{\sigma\,A_{\text{cond}}} \,,\tag{7}$$

where $A_{\text{cond}} = \pi\,D_{\text{cond}}^2/4$ is the cross-sectional area of the conductor with diameter D_{cond}, σ is the conductivity of the material, and L_{cable} is the total length of the cables used. The cable length depends strongly on the configuration, *i.e.*, where in the aircraft the motors and propulsors are placed in relation to the battery that supplies power to them. The method used to calculate the total wiring length for the reference aircraft is outlined in Sec. III.D.

The power dissipated in the cable can be calculated as

$$P_{\text{cable}} \;=\; I^2 R_{\text{cable}} \,.\tag{8}$$

4

This dissipated power, and thus the wasted energy, also has to be accounted for when sizing the battery and the thermal management system.

Each cable is composed of a conductor, assumed to be a solid cylinder, and the cylindrical shell insulation surrounding it. The mass of each part is then a product of the volume and the density ρ of the material. The mass of the wiring can thus be calculated as the sum of masses of the conductor and insulation, namely

$$
\begin{aligned}
m_{\text{wiring}} \quad &= \quad 1.2 \left(m_{\text{cond}} + m_{\text{ins}} \right) \\
&= \quad 1.2 \left(\frac{1}{4} \pi \rho_{\text{cond}} D_{\text{cond}}^2 L_{\text{cable}} + \frac{1}{4} \pi \rho_{\text{ins}} \left[\left(2\, t_i + D_{\text{cond}} \right)^2 - D_{\text{cond}}^2 \right] L_{\text{cable}} \right) ,
\end{aligned}
\tag{9}
$$

where the factor of 1.2 accounts for the mass of wire clamps, mounts, and other fixing components [11].

D. Thermal Management System (TMS)

Each component in the propulsion system operates at a certain efficiency, η, less than unity. The energy wasted is assumed to be dissipated as heat, necessitating a thermal management system that handles the wasted heat. The TMS is a heat exchanger that circulates wasted heat from all the electrical components, including the battery, electrical bus, converter, motor, and wiring, and cools these components during operations. The product of inefficiency of each component (defined as $1 - \eta$) and the input power to each component determines the wasted heat energy per unit time

$$
\dot{Q}_{\text{comp}} = (1 - \eta_{\text{comp}})\, P_{\text{comp,in}} .
\tag{10}
$$

The sum of the $\dot{Q}$ values from all the components then sizes the TMS.

The heat exchanger is modeled as having a hot side and a cold side separated by a wall, as shown in Fig. 2. The specific type modeled here is a compact double-pipe crossflow heat exchanger, where the hot side carrying waste heat from the electrical components in the propulsion system forms the inner pipe with the coolant flowing through it, and the cold side using air from the freestream forms the outer pipe, separated by a wall. Each part has an associated thermal resistance, $\mathscr{R}$. The following procedure to size the heat exchanger is derived using the number of thermal units (NTU) method outlined in [12], [13], and [14].

The basic equations that relate the heat transfer rate $\dot{Q}$ on each side are given as

$$
\dot{Q} = \dot{m}_h\, c_{p,h} \left(T_{\text{h,in}} - T_{\text{h,out}} \right),
\tag{11}
$$

$$
\dot{Q} = \dot{m}_c\, c_{p,c} \left(T_{\text{c,out}} - T_{\text{c,in}} \right),
\tag{12}
$$

where the subscripts 'h' and 'c' denote the hot and cold sides, $\dot{m}$ is the mass flow rate, c_p is the specific heat at constant pressure, and T is the temperature. The heat transfer rate can also be calculated as

$$
\dot{Q} = U_0\, A_0\, \Delta T_{\ell m},
\tag{13}
$$
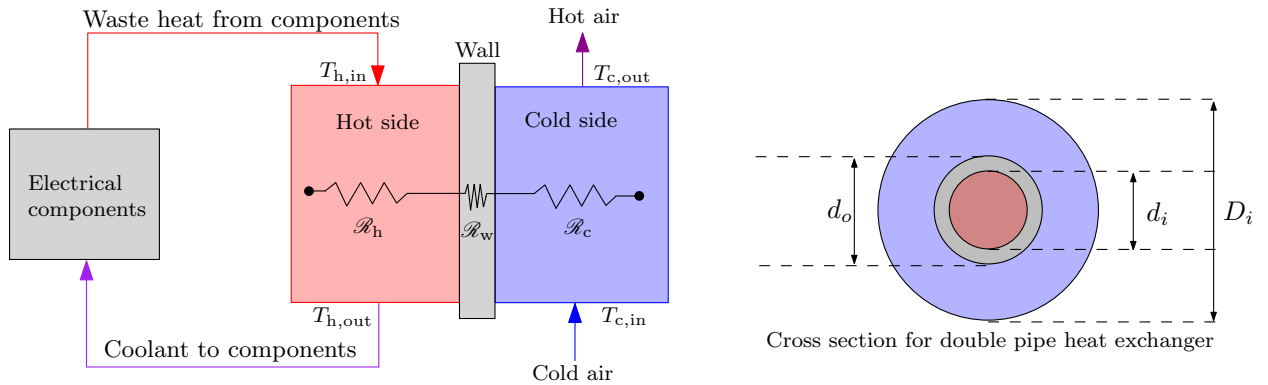
Fig. 2 Heat exchanger model.

where $A_0 = \pi\, d_o\, L_{\text{ex}}$ is the heat transfer surface area, L_{ex} is the length of the heat exchanger. The log mean temperature difference is given by

$$
\begin{aligned}
\Delta T_{\ell\text{m}} &= \frac{\Delta T_1 - \Delta T_2}{\ln\left(\Delta T_1/\Delta T_2\right)}\,, \\
\Delta T_1 &= T_{\text{h,in}} - T_{\text{c,out}}\,, \\
\Delta T_2 &= T_{\text{h,out}} - T_{\text{c,in}}\,,
\end{aligned}
$$

The overall heat transfer coefficient is calculated in terms of the thermal resistances of the hot side and the cold side (assuming wall thermal resistance to be negligible) as

$$
U_0 = \left(\mathcal{R}_h + \mathcal{R}_c\right)^{-1}\,, \tag{14}
$$

$$
\mathcal{R} = \frac{1}{\mathfrak{h}\, A_0}\,, \tag{15}
$$

where $\mathfrak{h}$ is the convection coefficient of heat transfer, which depends on the Nusselt number Nu, the thermal conductivity k, and the hydraulic diameter D_h as

$$
\mathfrak{h} = \frac{(\text{Nu})\, k}{D_h}\,. \tag{16}
$$

To size the heat exchanger for maximum waste heat rejection, it is assumed that the flow is turbulent, so that the Nusselt number can be calculated using the Dittus-Boelter equation:

$$
\text{Nusselt number:} \quad \text{Nu} = 0.023\, \text{Re}^{0.8}\, \text{Pr}^{0.4}\,, \tag{17}
$$

$$
\text{Reynolds number:} \quad \text{Re} = \frac{D_h\, G}{\mu}\,, \tag{18}
$$

$$
\text{Prandtl number:} \quad \text{Pr} = \frac{\mu\, c_p}{k}\,, \tag{19}
$$

where μ is the dynamic viscosity, $G = \dot{m}/A_c$ the flow mass velocity, and A_c the cross-sectional area. To complete the set of equations, the pressure loss is needed, which can be calculated as

$$
\Delta p = \frac{2\, \mathfrak{f}\, G^2\, L_{\text{pipes}}}{\rho\, D_h}\,, \tag{20}
$$

where ρ is the density of the fluid, L_{ex} is the length of the heat exchanger, and $\mathfrak{f}$ is the friction factor, which for turbulent flow can be estimated as

$$
\mathfrak{f} = 0.046\, \text{Re}^{-0.02}\,. \tag{21}
$$

The power needed to overcome this pressure loss can be calculated as

$$
P_{\text{pres}} = \frac{\dot{m}\, \Delta p}{\eta_{\text{pump}}\, \rho}\,, \tag{22}
$$

where η_{pump} is the efficiency of the pump, assumed to be 0.8 for this work. This power is assumed to be supplied from the battery.

The steps from Eq. (15) to (22) must be repeated for both the hot and the cold sides. Finally, the heat exchange between the hot side and the cold side is calculated in terms of the number of thermal units (NTU) as

$$
\text{NTU} = \frac{U_0\, A_0}{C_{\text{min}}}\,, \tag{23}
$$

where $C_{\text{min}} = \min\left(\dot{m}_h\, c_{p,h},\ \dot{m}_c\, c_{p,c}\right)$ is the minimum of the heat capacity rates; in this case, between the coolant and the air. Similarly, defining $C_{\text{max}} = \max\left(\dot{m}_h\, c_{p,h},\ \dot{m}_c\, c_{p,c}\right)$, the heat capacity ratio can be written as

$$
C_r = \frac{C_{\text{min}}}{C_{\text{max}}}\,, \tag{24}
$$

which can then be used to calculate the heat exchanger effectiveness

$$\epsilon \;=\; 1 - \exp\left[\left(\frac{1}{C_r}\right)\text{NTU}^{0.22}\left(\exp\left[-(C_r)\,\text{NTU}^{0.78}\right]-1\right)\right]. \tag{25}$$

Then, the actual heat transfer rate is calculated as

$$\dot{Q} \;=\; \epsilon\,C_{\min}\left(T_{h,\text{in}}-T_{c,\text{in}}\right). \tag{26}$$

This system of equations is solved to size the TMS in terms of the geometry (d_i, d_o, D_i, and L_{ex}) based on the ambient conditions, as well as limits on acceptable temperatures and pressure losses. The diameter of the inner pipe, d_i, which carries the coolant to and from the electrical components is also used to size the pipes needed for transport. The pipe network is assumed to consist of cylindrical pipes of inner diameter d_i and thickness t_{pipes}, such that the mass can be calculated as

$$m_{\text{pipes}} \;=\; 1.2\left(\frac{1}{4}\,\pi\,\rho_{\text{pipes}}\left[\left(d_i+2t_{\text{pipes}}\right)^2-d_i^2\right]L_{\text{pipes}} \;+\; \frac{1}{4}\,\pi\,\rho_{\text{coolant}}\,d_i^2\,L_{\text{pipes}}\right), \tag{27}$$

where L_{pipes} is the total length of the pipe network and ρ is the density. As with the wiring, the factor of 1.2 accounts for the mass of mounts and fixes required.

III. Modeling Framework and Reference Aircraft

A. Propulsion System

The all-electric propulsion system, shown in Fig 3, builds on the powertrain with its components (battery, converter, motor) from previous work [4], adding models for the propulsor, power distribution, thermal management system (TMS), and wiring (not shown in the schematic). Power (shown in blue) flows from the battery through the converter and power distribution system, then is distributed to the N_{prop} propulsors through an array of N_{prop} motors. For each component, the power it outputs to the next component is the product of its input power and efficiency. Whatever power it does not output is wasted as heat. The power flow equations are described in previous work [4] and will not be repeated here.

The heat flow lines (in red) connect each component ultimately to the TMS, which is a heat exchanger and thus cools the components. Note that the placement of the heat flow arrows are intended for illustrative purposes only. The optimality of heat exchanger flow paths are beyond the scope of this work. In addition, wiring and TMS piping are not shown in the schematic; however, the weight of both are also taken into account in the analysis.

B. Component Sizing

Components are sized based on the power flows that they handle. In general, the mass of each component is calculated as follows:

$$m_{\text{comp}} = P_{\text{comp}} \,/\, \text{SP}_{\text{comp}}, \tag{28}$$
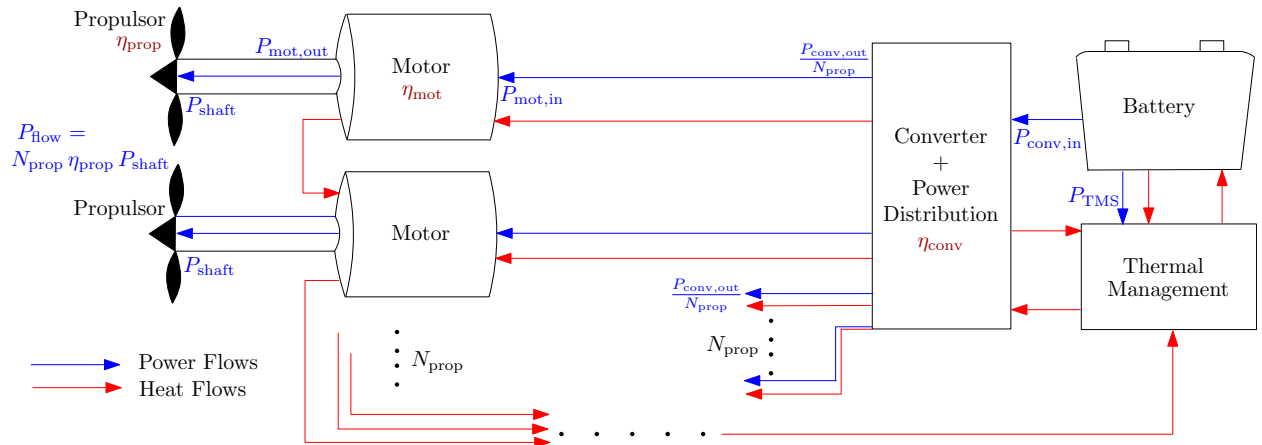
Fig. 3   Propulsion system schematic.

7

where P_{comp} is the output power of the component, and SP_{comp} is the specific power, or power per unit mass, of the component, obtained from technology scenarios expected in the 2035 timeline [4]. For the TMS, numbers quoted in literature sometimes use the inverse of specific power [15], or the mass per rejected heat energy per unit time. Where appropriate, these alternative numbers have been used in place of specific power to size components. The wiring and TMS piping masses are calculated directly from the volume sizing and the materials used in both.

C. Technology Assumptions

Table 1 summarizes the technology scenario used here to size the components in terms of mass. A detailed discussion behind the rationale for using these values can be found in previous works [1, 2]. Compared with previous work, the new additional parameter is the specific power for the thermal management system, obtained from [15].

D. Aircraft and Mission

Previous results [1, 2] showed that all-electric power system architectures will only be feasible for small aircraft flying short missions in the near future, the representative mission studied here is that of a commuter aircraft (modeled on the Viking Air Twin Otter), with the relevant mission parameters given in Table 2. These parameters were used to construct a mission power profile for the Twin Otter [4], as well as to calibrate parameters related to distributed propulsion. For example, for a case of 10 propulsors versus the two on the Twin Otter, the total fan area was kept constant. The smaller diameters for the 10 propellers were calculated meet this requirement.

For configuration-specific calculations like the length of the wiring, the Twin Otter fuselage was modeled as having an ellipsoidal cross-section, as seen in Fig. 4. The battery and power distribution system are assumed to be placed below the passenger cabin at the bottom part of the fuselage. From there, the wires travel along the fuselage sidewalls and the wing to transfer power to the motor-propulsor arrays distributed over the wingspan. The wiring is assumed to be contained in the same plane as the cross-section shown in Fig. 4, *i.e.* the distances that arise from the distribution system

Table 1 Technology scenarios: assumptions values for electrical component parameters.

Parameter	Units	Expected 2035 Value
Pack Battery Specific Energy (BSE)	W·h/kg	575
Motor Specific Power (SP)	kW/kg	12
Converter SP	kW/kg	14
Thermal Management System SP	kW/kg	0.68

Table 2 Baseline aircraft and mission specifications [16]

		Twin Otter
Number of passengers	N_{pax}	19
Payload	m_{pay}	1 842 kg
Mission range	R	100 nmi (185 km)
Cruise speed	V_{cruise}	94 m/s
Takeoff mass	m_{TO}	5 670 kg
Fuselage height	h_{fuse}	2.09 m
Fuselage width	w_{fuse}	1.75 m
Propeller diameter	D_{prop}	2.6 m
Number of blades per propeller	B_{prop}	3
Cruise lift-to-drag ratio	$(L/D)_{\text{cruise}}$	12
Cruise altitude	h_{cruise}	10,000 ft (3,050 m)
Service ceiling	h_{SC}	27,600 ft (8,138 m)
Max rate of climb	$\dot{h}_{\text{max}}$	490 m/min
Climb gradient	dh/dR	107 m/km
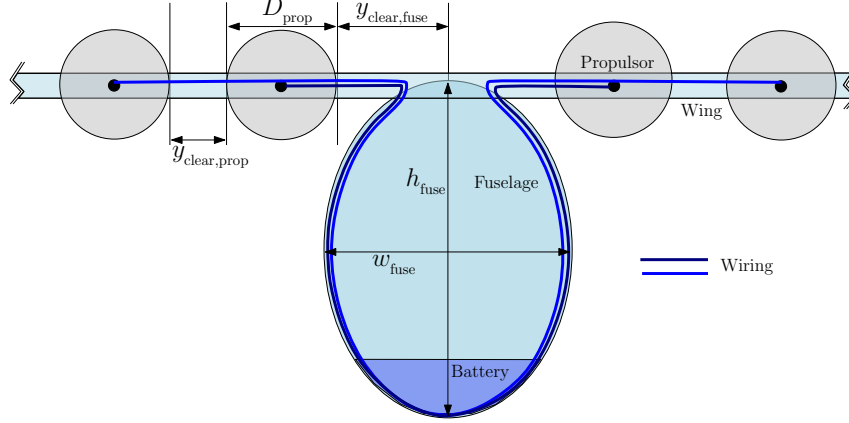
Fig. 4 Twin Otter cross-section schematic to calulate wiring length.

not being in the same plane as the motors are neglected. For a system with N_{prop} propulsors spread symmetrically throughout the wingspan, the length of the wiring can be calulated as

$$L_{\text{cable}} \;=\; 4 \left[N_{\text{prop}} \left(C_{\text{fuse}} + y_{\text{clear,fuse}} \right) + 2 \sum_{k=1}^{\frac{1}{2}N_{\text{prop}}} \left[\left(k - \frac{1}{2} \right) D_{\text{prop}} + (k-1) y_{\text{clear,prop}} \right] \right], \tag{29}$$

where the factor of 4 accounts for there being 4 wires ($\pm V/2$ and a ground for each) for a DC power distribution system. $y_{\text{clear,prop}}$ is the distance between the blade span of two adjacent propellers, and $y_{\text{clear,fuse}}$ is the clearance between the fuselage and the propulsor, set to half the fuselage width plus $y_{\text{clear,prop}}$. D_{prop} is the diameter of each propulsor. The circumference of the fuselage cross-section, assumed to be an ellipse, is calculated as [17]

$$C_{\text{fuse}} \;=\; \pi\,(a+b) \left[1 + \frac{3h}{10 + \sqrt{4-3h}} \right], \tag{30}$$

$$h \;=\; \frac{(a-b)^2}{(a+b)^2},$$

where $a = \frac{1}{2}h_{\text{fuse}}$, and $b = \frac{1}{2}w_{\text{fuse}}$ are the semi-major and semi-minor axes of the ellipse, respectively.

To calculate the overall length of the pipe network that recirculates coolant between the thermal management system and the motors, the same approach is used, except only two pipelines are needed – to transport coolant to and from the motors. As a result, the length of the pipes needed is $L_{\text{pipes}} = L_{\text{cable}}/2$, since the total length of the cables assumes four cables per line.

IV. Results

The propulsion system in Fig. 3 is simulated using the power profile generated from the aircraft mission of Sec. III.D. The following results are divided into two parts: the first looks at subsystem-level studies for the power distribution, wiring, and thermal management; and the second considers at aircraft-level studies. At the aircraft level, the results show a mass breakdown of the propulsion system by component, as well as the effects of distributed propulsion on the mass of the propulsion system and its components.

A. Subsystem-Level Studies

1. Power Distribution

Equation (3) in Section II.B describes the relationship between the breakdown voltage and the product of air pressure and separation between electrodes. This product pd does not provide an intuitive way of understanding the effects that pressure and separation individually have on the breakdown voltage. Figure 5(a) shows the effect when pressure and
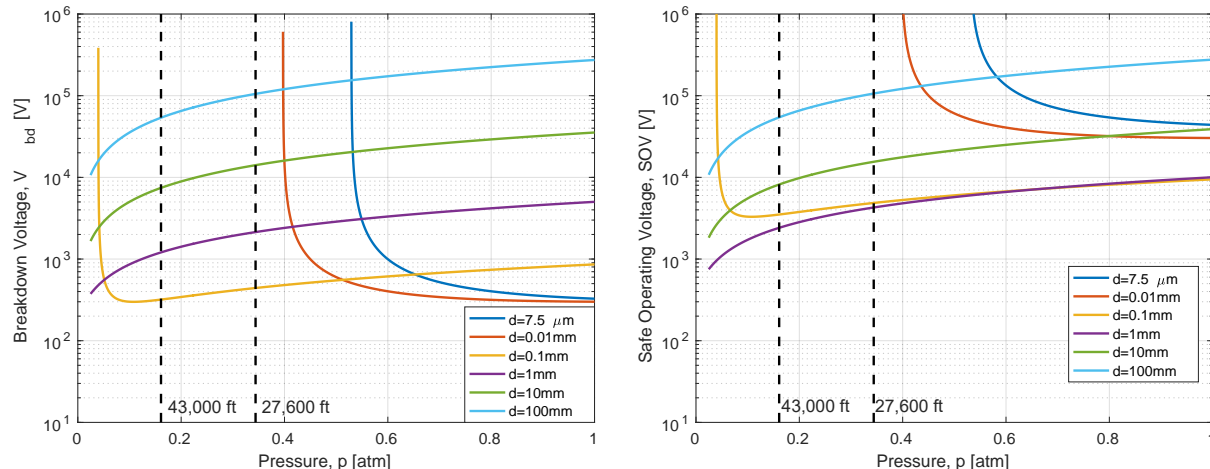
Fig. 5 (*a*) **Variation of breakdown voltage for uninsulated conductors, and** (*b*) **variation of safe operating voltage (SOV) for insulated conductors at different pressures and conductor spacing.**

separation are decoupled. This result is valid for uninsulated conductors given by Eqn. (3). As seen for very small spacings ($d \leq 0.1$ mm), the breakdown voltage first drops sharply, reaching a minimum, then increases gradually with pressure. For larger gap lengths ($d \geq 1$ mm), this effect is present but cannot be seen in the plots, as the lowest value pressure used was that corresponding to the US Standard Atmosphere at an altitude of 25 km, where the isothermal layer ends in the stratosphere, and well beyond the 43,000 ft (13.1 km) maximum altitude current commercial aircraft fly at. At 43,000 ft, for example, the breakdown voltage is 1.2 kV for a separation of 1 mm, about four times the 327 V minimum breakdown voltage for any combination of p times d. At the 27,600-ft service ceiling of the reference Twin Otter aircraft, the breakdown voltage is 2.1 kV at $d = 1$ mm.

When wires are modeled with insulation, as in real-world applications, the safe operating voltage is considered instead of the breakdown voltage, as indicated in Eqns.(4) and (5). Figure 5(b) shows how the safe operating voltage (SOV) as the separation between the conductors varies when the conductors are insulated. The trends are similar to the uninsulated case, but the safe operating voltages are higher than the corresponding breakdown voltages. For a separation of 1 mm, the safe operating voltage increases to 2.4 kV at 43,000 ft and to 4.3 kV at 27,600 ft.

For the previous studies, the insulation thickness and the material were kept constant. Figure 6 shows the effects of varying the thickness t_i (a), and insulation material, represented by dielectric constant ε_r (b). The ranges for t_i were determined from the appropriate thicknesses based on the American Wire Standard wire gauges as presented in [6], and those for ε_r were based on the different insulating materials used for commercial conducting wires[18]. Across the ranges considered, the SOV increases with increasing pressure while varying both t_i and ε_r. To increase SOV, the insulation thickness must be increased and a material with a lower dielectric constant must be used. The effects of both, however, pale in comparison to the effect of increasing the separation between the conductors. In addition, the types and thicknesses of insulation used in standard wiring are not expected to change drastically, so any gains for SOV must come from separation between conductors only, assuming electrified aircraft are expected to be certified to the same service ceiling (hence, pressure/altitude) as current aircraft.

Consider some point analyses for current aircraft. As a reasonable case, the wires are assumed to be insulated with polyethylene ($\varepsilon_r = 2.28$) with an insulation thickness of $t_i = 1$ mm and a conductor spacing of at least $d = 2$ mm. Table 3 shows the results of safe operating voltage calculations for different aircraft classes. For a long range aircraft with a service ceiling of 43,000 ft, the SOV is 2.47 kV. Applying a safety factor of 1.5 reduces this to 1.65 kV. For the commuter Twin Otter-like aircraft with a service ceiling of 27,600 ft, the SOV is 4.52 kV and is reduced to 3.01 kV with a 1.5 safety factor. This analysis shows that SOV for aircraft can be much higher than the minimum predicted by Paschen's Law after accounting for insulation and conductor spacing, even at the altitudes aircraft fly at. All of these values fall under the 4.5 kV high-voltage architectures supported by the NASA Electric Aircraft Testbed (NEAT) [19]. For the all-electric commuter aircraft analyzed in this work, a SOV of 3 kV will be used.
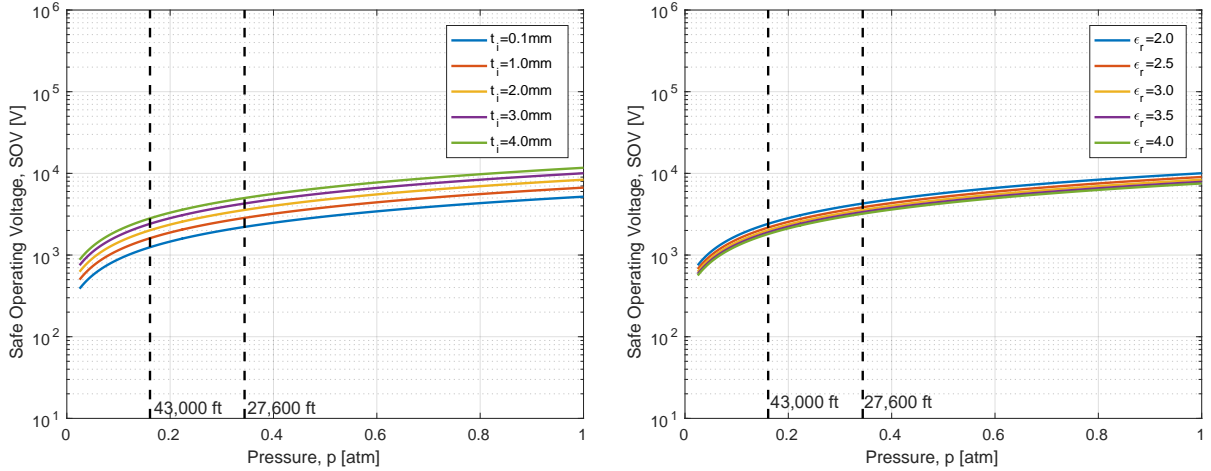
Fig. 6 (*a*) **Variation of safe operating voltage (SOV) with insulation thickness, and (*b*) with insulation material at different pressures.**

Table 3 Safe operating voltages for different aircraft classes at different safety factors.

Class of Aircraft	Example	Service ceiling [ft]	Safe Operating Voltage (SOV) [kV]	SOV [kV] Safety factor 1.2×	SOV [kV] 1.5×
Long-range	777, A350	43,000	2.47	2.06	1.65
Commuter	Twin Otter	27,600	4.52	3.77	3.01

2. Wiring

Using the power required by each motor-propulsor array, the electrical conductors for a four-wire DC transmission system are sized. The length of the wiring required for a Twin Otter-like commuter aircraft is calculated using the method in Sec. III.D. The wire gauge required, as well as the resistance, power loss, and mass are all calculated using the equations in Sec. II.C. For the Twin Otter mission, the maximum power required is about 990 kW at cruise [4].

Table 4 shows point design studies for wiring. For 2 propulsors, the wiring length is considerably shorter compared to that for 20 propulsors, but the wires themselves are thicker to handle the larger currents. As a result, despite the large difference in wiring lengths for the two cases, the total wiring mass is comparable. However, compared to the overall propulsion system mass of about 1400 kg, the wiring mass is negligible, even for 20 propulsors. In terms of power losses, all four cases considered result in a wiring efficiency of over 99%, *i.e.* the power lost in the cables is negligible compared to the climb power required. The material used also makes little difference: using copper results in lower power losses at the penalty of being heavier; however, compared to the masses and power of other components in the propulsion system, the choice of material for wiring makes little difference. Copper wires are chosen for all subsequent analyses.

Table 4 Wiring resistance, mass, and power for copper and aluminum conductors for 2 and 20 propulsors.

Number of Propulsors	Current I [A]	Conductor Diameter D_{cond} [mm]	Wiring Length L_{cable} [m]	Material	Resistance R_{cable} [Ω]	Total Mass m_{cable} [kg]	Power Loss P_{cable} [kW]
2	165	6.5	42	Copper	0.07	16	1.82
				Aluminum	0.11	6	2.86
20	17	1.6	627	Copper	16.43	19	4.47
				Aluminum	25.97	10	7.07

11

It should be noted here that these analyses were done using the 3 kV safe operating voltage identified at the beginning of this section. Lower voltages could be used for power distribution, with the current subsequently increasing, but this would result in higher masses and power losses in the wiring. The mass is proportional to the square of the conductor diameter, which is sized by the maximum current rating. Power losses scale with the square of the current. Increased power losses also require a larger battery to supply extra power to overcome those losses. Therefore, for efficient, lightweight power distribution, high voltage and low current provide the best results. An alternative would be to use superconducting cables with very low resistances, allowing much higher currents and low voltages. However, a cryocooler would be needed to cool the conductors to the extremely low temperatures required. Superconductivity would add a layer of complexity to the modeling and is beyond the scope of this work.

3. Thermal Management Network of Pipes

The thermal management system (TMS) is sized based on the total heat to be rejected from the electrical components. The pipes carrying the coolant to each component have to be sized. The hydraulic diameter is calculated based on the TMS sizing from Sec. II.B and the length of the pipes from Sec. III.D. The coolant is assumed to be propylene glycol and the pipes are assumed to be made up of aluminum, based on the cooling system for the Boeing 787 electronics [20].

For the heat exchanger, the air acting as the cold side fluid was assumed to enter at ambient temperature at the flight segment and assumed to exit at a maximum temperature of standard sea-level (SLS) conditions, or 288 K. For the glycol acting as the hot side fluid, the temperature at the inlet was determined from the model and the exit temperature was limited to 273 K. For this work, it is assumed that there is no heat lost during transport from the component to the heat exchanger; for example, if the motor temperature was T_{mot}, then this is assumed to be the temperature of the glycol entering the heat exchanger.

Similar to the previous analyses, the sizing of the thermal management was done for 2 and 20 propulsors. For both cases, the climb segment resulted in the largest amount of heat lost. The motors were most efficient at climb, for which they were optimized; however, since climb requires about twice the cruise power and about six times the approach power, the power loss was still the highest at climb. So the total power loss during climb was used to size the heat exchanger. Table 5 shows the results. Going from 2 to 20 propulsors, the power loss increases by about 10% due to the motor iron losses constituting a larger fraction of total losses, which adds up over 20 motors. The pipes themselves are smaller; however, the network of pipes is much longer overall. The longer pipes, combined with more heat to be rejected, results in a larger total pipe mass for 20 propulsors. However, the total pipe mass, like the total wiring mass, represents a minuscule fraction of the overall propulsion system weight. Comparatively, the heat exchanger had a mass of 107 kg and 127 kg for 2 and 20 propulsors respectively.

It should be noted that the pipe network is very configuration-dependent. This example assumed there was a central TMS that rejected heat from all the electrical components, whereas for increased distribution, it might make sense in terms of complexity and weight to cool the motors, drawing air directly from the freestream instead of using a centralized TMS.

Table 5   Thermal management pipe network properties

Number of Propulsors	Power Loss $\dot{Q}$ [kW]	Hydraulic Diameter d_i [mm]	Total Pipe Length L_{pipes} [m]	Total Pipe Mass m_{pipes} [kg]
2	63	79	21	15
20	70	8	315	24

B. Aircraft-Level Studies

1. System Mass Breakdown

Figure 7 shows the mass breakdown of the propulsion system for different numbers of propulsors: two propulsors on the left and 20 on the right. For both cases, the battery accounts for over 60% of the system mass, with the next largest contribution coming from the propulsors. This result indicates that the battery gains the most from technological advances of specific energy and specific power. The other components gain relatively less from advances in specific
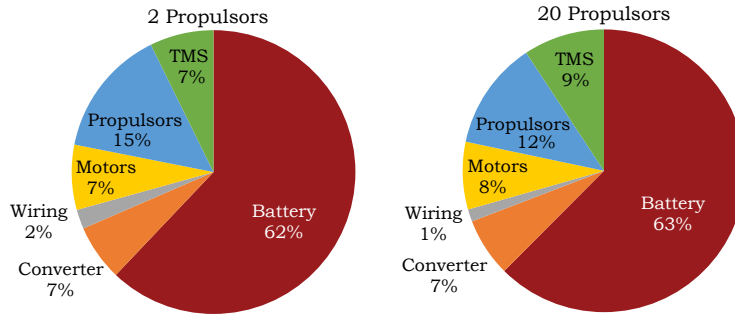
Fig. 7 Propulsion system mass breakdown by component for (left) two propulsors and (right) 20 propulsors.

power; however, their efficiencies affect the battery sizing as well. Therefore, other components can afford to add mass if it improves their efficiency.

The motors and converter each account for less than 10% of the propulsion system mass. For 20 propulsors, the fraction of the propulsor mass goes down, due to the benefits of the cube-squared law of mass to propulsive power scaling. The mass scales with the volume of the propulsor (volume ~ characteristic length cubed) whereas the power, from the product of thrust and flight speed, scales with the fan area (area ~ length squared). For the same total fan area as prescribed in this analysis, 20 smaller propulsors collectively weigh less than the two larger ones. In addition, for 20 propulsors, even though the battery represents a slightly larger fraction of the system mass, the actual mass of the battery goes down, in part due to the mass of the propulsors going down. In each case, the wiring accounts for a tiny fraction of the overall propulsion system mass, whereas the thermal management system and associated piping accounts for a significant part of the total mass. The TMS increases in both actual mass and as a fraction of the total mass, due to the need for cooling an increased number of motors.

In terms of actual mass, the propulsion system with 20 propulsors weighs 1,372 kg, about 6% less than the propulsion system with 2 propulsors, which is a meaningful difference. The mass of the propulsors going down directly contributes to the mass of the overall propulsion system going down with increased distribution. The next section looks at the effects of distribution in more detail.

2. Distributed Propulsion

Figure 8 tracks the component masses as the number of propulsors is varied from 2 to 20. The plot on the left shows the masses of all components, including the total propulsion system mass in black, and the plot on the right zooms in on the smaller components to provide more detail. The overall mass of the propulsion system decreases with more distribution by about 6% going from 2 to 20 propulsors. The motor and converter masses stay roughly flat, whereas the thermal management system mass increases with more distribution. The invariance in converter mass can be explained by the fact that there is one converter that supplies power to the motors and acts as the power distribution system; therefore, as long as the total flow power needed remains constant irrespective of the number of propulsors, the size of the converter also does not change. In addition, both the motor and the converter are optimized in each case. In particular, the motor efficiency remains roughly constant whether the motor is sized for half of the flow power needed (2 propulsors) or for $1/20^{\text{th}}$ (20 propulsors).

In contrast, distribution lowers the mass of the propulsors more significantly and the overall system mass decreases with more distribution. However, as the number of propulsors is increased further, the effect diminishes, largely due to the increased mass of thermal management system (TMS) required to deliver cooling to the increased number of motors. For 20 smaller motors versus 2 larger ones, the iron losses in the motor remain constant while the resistive losses decrease; as a result, the power loss of each motor is a larger fraction of the output power. Collectively across 20 motors, this means more total heat has to be rejected, requiring a larger TMS. Therefore, with 20 propulsors, the weight savings from the smaller propulsors fail to provide overall system weight benefits compared with 10 propulsors.

13
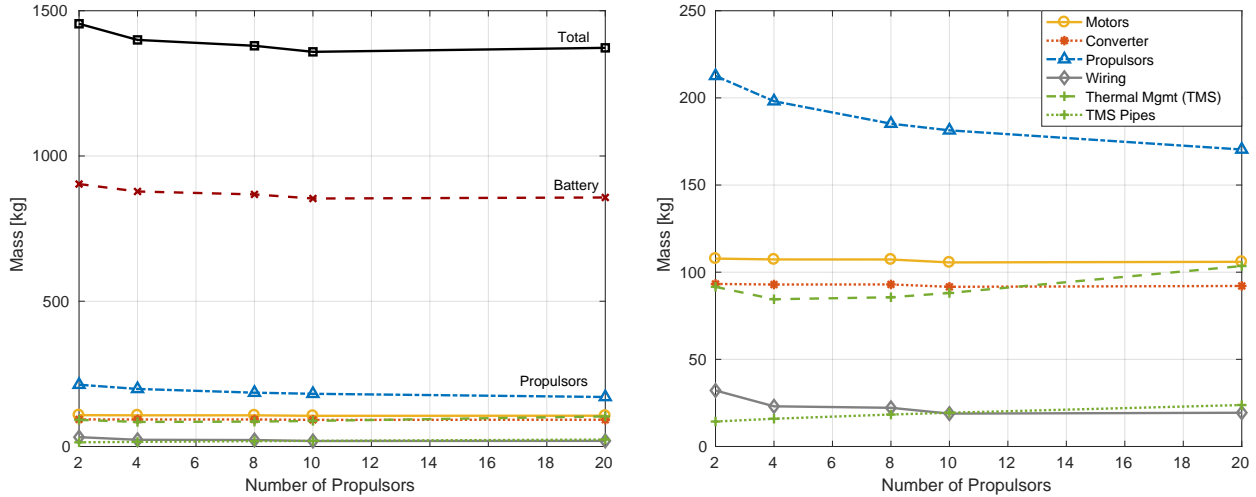
Fig. 8 Propulsion system mass changes with distributed propulsion; *(left)* **showing all the components, and** *(right)* **showing more detail of the smaller components.**

C. Limitations and Future Work

The major limitation of this work is that it looks at the propulsion system for an all-electric aircraft in isolation without considering the other aspects of aircraft sizing - fuselage, wings, and so on. The power profile of a commuter aircraft is used to size the electrical components needed to provide that power at expected 2035 technology levels. However, the sizing of electrical components does not then iteratively resize the aircraft. For example, the maximum takeoff mass (MTOM) of the baseline Twin Otter is 5,670 kg and the payload is 1,842 kg (19 passengers) over a 100-nmi mission. For the all-electric aircraft with two propulsors, the mass of the propulsion system only is 1,455 kg, or about 25% of the MTOM of the Twin Otter. To gain a more complete picture of how much the all-electric aircraft would weigh, this propulsion system mass has to be used to iteratively resize the aircraft and compute a new MTOM. In other words, the component models and propulsion system presented in previous [4] and this work lack integration with an overall aircraft sizing tool that incorporate other aspects of aircraft design. Integrating this propulsion system framework into an aircraft sizing tool to look at aircraft-level results would be the primary goal of future work.

Additionally, this work did not consider the volume constraints of the components, specifically the wiring and the thermal management with its network of pipes. These two details are rather configuration-specific, and given the focus on the performance of electrical components during flight loads, was outside the scope of this work. That being said, to present a complete picture, a volume analysis will be done to ensure that the components as sized will fit in the basic geometry of the reference aircraft. Other limitations include the focus on commuter aircraft like the Twin Otter with a payload of 19 passengers, and the focus on an all-electric propulsion system. Previous work [1, 2] showed promise for hybrid- and turbo-electric aircraft for larger classes flying longer missions, and the aim is to extend this framework to cover those areas of the design space as well.

V. Summary and Conclusions

This paper presents models for components of an all-electric propulsion system, including the power distribution system, thermal management system, wiring, and propulsor. Together with the powertrain components modeled in previous work [4], these constitute a comprehensive all-electric propulsion system framework. It captures the operational behavior exhibited by electrical components under variable power loads representative of different flight segments.

Applying this framework to a mission representative of a commuter aircraft shows that the battery dominates the mass breakdown of the propulsion system, accounting for over 60% of the propulsion system mass. While none of the other components amount to more than 15% each by mass, their inefficiencies play a significant role in battery sizing, as the battery has to compensate for the component losses.

Distributed propulsion is found to provides system weight savings. However, with increased distribution levels,

14

the benefits fail to compensate for the larger size of the thermal management system needed to cool a larger number of motors. The benefits of distributed propulsion therefore diminish with increased distribution. Specifically, going beyond 10 propulsors does not result in a meaningful reduction of propulsion system mass.

References

[1] Kruger, M., Byahut, S., Uranga, A., Dowdle, A., Gonzalez, J., and Hall, D. K., "Electrified Aircraft Trade-Space Exploration," AIAA 2018-4227, 2018 AIAA Aviation, Atlanta, GA, 25–29 June, 2018. doi:10.2514/6.2018-4227.

[2] Hall, D., Greitzer, E., Dowdle, A., Gonzalez, J., Hoburg, W., Lang, J., Sabnis, J., Spakovszky, Z., Yutko, B., Courtin, C., Thalheimer, W., Trollinger, L., Tylko, J., Varney, N., Uranga, A., Byahut, S., and Kruger, M., "Feasibility of Electrified Propulsion for Ultra-Efficient Commercial Aircraft, Final Report," NASA/CR—2019-220382, 2018.

[3] Moore, M. D., and Fredericks, B., "Misconceptions of electric propulsion aircraft and their emergent aviation markets," AIAA 2014-0535, 2014 AIAA SciTech, National Harbour, MD, 13–17 Jan., 2014. doi:10.2514/6.2014-0525.

[4] Byahut, S., and Uranga, A., "Propulsion Powertrain Component Modeling for an All-Electric Aircraft Mission," AIAA 2020-0015, 2020 AIAA SciTech, Orlando, FL, 6–10 January, 2020. doi:10.2514/6.2020-0015.

[5] Torenbeek, E., *Advanced Aircraft Design: Conceptual Design, Technology and Optimization of Subsonic Civil Airplanes*, John Wiley & Sons, 2013.

[6] Christou, I., Nelms, A., Cotton, I., and Husband, M., "Choice of optimal voltage for more electric aircraft wiring systems," *IET Electrical Systems in Transportation*, Vol. 1, No. 1, 2011, pp. 24–30. doi:10.1049/iet-est.2010.0021.

[7] Husain, E., and Nema, R. S., "Analysis of Paschen Curves for air, N2 and SF6 Using the Townsend Breakdown Equation," *IEEE Transactions on Electrical Insulation*, Vol. EI-17, No. 4, 1982, pp. 350–353. doi:10.1109/TEI.1982.298506.

[8] Armstrong, M. J., Blackwelder, M., Bollman, A., Ross, C., Campbell, A., Jones, C., and Norman, P., "Architecture, Voltage, and Components for a Turboelectric Distributed Propulsion Electric Grid (Final Report)," NASA/CR—2015-218440, 2015. Accessed: 07/08/2020.

[9] European Union Aviation Safety Agency (EASA), "Airbus A350 Type-Certificate Data Sheet," `https://www.easa.europa.eu/sites/default/files/dfu/TCDS_EASA%20_A_151_Airbus350_Iss22-2019-11-27.pdf`, 2019. Accessed: 07/08/2020.

[10] Farr, H. H., *Transmission Line Design Manual*, United States Department of the Interior Water and Power Resources Service, 1980.

[11] Doering, R., and Thielecke, F., "An Evaluation of the Potential of Local Electric Power Packages on Aircraft Fleet Level," AIAA 2019-2804, 2019 AIAA Aviation Forum, Dallas, TX, 17–21 January, 2019. doi:10.2514/6.2019-2804.

[12] Chapman, J. W., Schnulo, S. L., and Nitzsche, M. P., "Development of a Thermal Management System for Electrified Aircraft," AIAA 2020-0015, 2020 AIAA SciTech, Orlando, FL, 6–10 January, 2020. doi:10.2514/6.2020-0545.

[13] Hesselgreaves, J., *Compact Heat Exchangers: Selection, Design, and Operation*, Elsevier Science & Technology Books, 2001.

[14] Lee, H., *Thermal Design: Heat Sinks, Thermoelectrics, Heat Pipes, Compact Heat Exchangers, and Solar Cells*, John Wiley & Sons, Inc., 2010.

[15] Welstead, J., and Felder, J., "Conceptual Design of a Single-Aisle Turboelectric Commercial Transport with Fuselage Boundary Layer Ingestion," AIAA 2016-1027, 2016 AIAA SciTech, San Diego, CA, 4–8 January, 2016. doi:10.2514/6.2016-1028.

[16] Viking Air Ltd., "Viking Twin Otter Series 400 Technical Specifications and Standard Equipment List," , 2016.

[17] Ramanujan, S., Hardy, G., Aiyar, P., and Wilson, B., *Collected Papers of Srinivasa Ramanujan*, Cambridge University Press, 2015.

[18] Bernstein, B. S., "Electrical Properties of Cable Insulation Materials (Presentation)," `https://www.pesicc.org/iccWebSite/subcommittees/E/E04/2001/f2001_bernstein.pdf`, 2001. Accessed: 07/08/2020.

[19] Jansen, R. H., Bowman, C., Jankovsky, A., Dyson, R., and Felder, J., "Overview of NASA Electrified Aircraft Propulsion Research for Large Subsonic Transports," AIAA 2017-4701, 2017 AIAA Propulsion and Energy Forum, Atlanta, GA, 10–12 July, 2017. doi:10.2514/6.2017-4701.

[20] PTI Technologies Inc., "Cooling Flight Critical Electronics (Web Page)," `https://www.ptitechnologies.com/cooling-flight-critical-electronics/`, 2020. Accessed: 07/08/2020.